Ferroelectrics

ISSN: (Print) (Online) Journal homepage: https://www.tandfonline.com/loi/gfer20

Phase transition, microstructure and electrical properties of $Pb_{1-x}Y_{x/2}Bi_{x/2}[(Zr_{0.53}\ Ti_{0.47})_{0.92}–(Mn_{1/3}\ Sb_{2/3})_{0.08}]O_3$ piezoelectric ceramics

Sabrina Benseghir, Fares Kahoul, Louanes Hamzioui & Michel Aillerie

To cite this article: Sabrina Benseghir, Fares Kahoul, Louanes Hamzioui & Michel Aillerie (2021) Phase transition, microstructure and electrical properties of $Pb_{1-x}Y_{x/2}Bi_{x/2}[(Zr_{0.53}\ Ti_{0.47})_{0.92}–(Mn_{1/3}\ Sb_{2/3})_{0.08}]O_3$ piezoelectric ceramics, Ferroelectrics, 584:1, 198-211, DOI: 10.1080/00150193.2021.1984780

To link to this article: https://doi.org/10.1080/00150193.2021.1984780

Published online: 08 Dec 2021.

FERROELECTRICS
2021, VOL. 584, 198–211
https://doi.org/10.1080/00150193.2021.1984780

Taylor & Francis
Taylor & Francis Group

Phase transition, microstructure and electrical properties of $Pb_{1-x}Y_{x/2}Bi_{x/2}[(Zr_{0.53}\ Ti_{0.47})_{0.92}–(Mn_{1/3}\ Sb_{2/3})_{0.08}]O_3$ piezoelectric ceramics

Sabrina Benseghir[a], Fares Kahoul[b,c], Louanes Hamzioui[b,c], and Michel Aillerie[d,e]

[a]Interaction et Réactivité des Systèmes, Département Génie des Procédés, Laboratoire de Dynamique, Université de Ouargla, Ouargla, Algérie; [b]Département Socle Commun ST, Faculté de Technologie, Université de M'Sila, M'Sila, Algérie; [c]Département de Chimie, Laboratoire de Chimie Appliquée, Université de Biskra, Biskra, Algérie; [d]LMOPS, Université de Lorraine, Metz, France; [e]LMOPS, Centrale Supelec, Metz, France

ABSTRACT

Ceramics in PYBZT-PMS system with formula $Pb_{1-x}Y_{x/2}Bi_{x/2}[(Zr_{0.53}\ Ti_{0.47})_{0.92}–(Mn_{1/3}\ Sb_{2/3})_{0.08}]O_3$ (x = 0–0.00625) were prepared by the conventional solid state sintering. The evolution of microstructure and corresponding electrical properties of PYBZT-PMS samples were systematically studied. Phase transition from rhombohedral to tetragonal structure was identified by Raman spectra and XRD results, and the coexistence of two phases was observed near the composition range from x = 0.0025 to 0.005. Scanning electron micrographs of the samples show uniform distribution of grain and grain boundaries. The optimum electrical properties of PYBZT-PMS such as ε_r = 1119.397, $\tan\delta = 0.01535$, T_c = 390 °C, $\rho = 7.82\ g/cm^3$, $\sigma = 0.709\ (Mohm\ m)^{-1}$, Q_m = 525.232, and K_P = 0.639 were obtained at x = 0.00375.

ARTICLE HISTORY
Received 18 June 2021
Accepted 4 September 2021

KEYWORDS
Ceramics; MPB; ε_r; K_P; Q_m

1. Introduction

Lead zirconate titanate based perovskites (ABO_3) piezoelectric ceramics are widely used in various fields such as actuators, sensors, transducers, dynamic random access memory (DRAM), multi-capacitors, etc. due to their excellent piezoelectric properties [1–6].

The $Pb(Zr_xTi_{1-x})O_3$ (PZT) system and its modified solid solutions are known to exhibit excellent dielectric, elastic and piezoelectric properties at the morphotropic phase boundary (MPB) at which the tetragonal and rhombohedral phases coexist [5, 7–23]. In the vicinity of the MPB region, the six domain states of the tetragonal structure along the (100) direction (90° and 180° domains) symmetry coexist with the eight domain states of the rhombohedral along (111) directions (71°, 90° and 180° domains) symmetry. This results in 14 possible available directions of spontaneous polarization. All of the aforementioned factors make the properties show a maximum around the MPB [24, 25]. PZT series near the MPB have been found exhibiting outstanding piezoelectric, ferroelectric properties, excellent electromechanical coupling coefficient (K_p), mechanical

CONTACT Sabrina Benseghir ben_bina@hotmail.fr

quality factor (Q_m), temperature and time stabilities, which has established PZT itself as a great function electronics in modern materials science of electronic composites [26].

The physical properties of PZT ceramics can be modified by doping A-site (Pb) and B-site (Zr/Ti). By introducing various dopants or adding other component to the PZT, piezoelectric and dielectric properties can be tailored to a wide extent [15, 27–30]. One of the ways of improving the physical properties of PZT is adding donor/acceptor dopants that control the "hard" and "soft" behavior [31–33]. The main difference between "hard" and "soft" behavior of PZT originates from the polarization and depolarization behavior, mobility of domains and nature of dopants. PZT-hard is obtained by doping acceptor dopants such as K^+, Na^+ (for A site) and Fe^{3+}, Mn^{3+} (for B site), which reduces the domain mobility [1]. In case of PZT-soft, donor dopants such as La^{3+}, W^{6+} (for A site) and Nb^{5+}, Sb^{5+} (for B site) are added, which increase the domain mobility and ease of polarization [34].

It is well known that the piezoelectric properties of electro-ceramics depend on many factors, such as the composition of ceramics, processing techniques, MPB conditions [35–37], grain sizes [38, 39], poling conditions [25, 40, 41], etc. The effect of microstructure on electrical properties of the electro-ceramics is also reported by many researchers [42–44] Studies show that in the vicinity of the MPB, different ceramic materials have outstanding piezoelectric properties, which can be attributed to the unique structural features of the coexistence of tetragonal and rhombohedral phases with highest available directions of spontaneous polarization [45].

Zhu et al. [46] reported the presence of an additional increment in the piezoelectric response of $0.05Pb(Mn_{1/3}Sb_{2/3})O_3$-$0.95Pb(Zr_{0.52}Ti_{0.48})O_3$ (PMS-PZT) ceramics (showed high piezoelectric strain coefficient, planar electromechanical coupling, and dielectric constant, as well as low tangent loss with high Curie temperature for this ceramics).

In this work, we studied the effects of Y, and Bi addition on the phase structure, morphology, piezoelectric and dielectric properties of $Pb_{1-x}Y_{x/2}Bi_{x/2}[(Zr_{0.53}Ti_{0.47})_{0.92}$–$(Mn_{1/3}\ Sb_{2/3})_{0.08}]O_3$ ceramics.

2. Experimental procedures

Series of $Pb_{1-x}Y_{x/2}Bi_{x/2}[(Zr_{0.53}\ Ti_{0.47})_{0.92}$–$(Mn_{1/3}\ Sb_{2/3})_{0.08}]O_3$ ceramics (with $x = 0$, 0.00125, 0.0025, 0.00375, 0.005 and 0.00625) are prepared by the conventional mixed oxide process. Ceramics specimens with various compositions were prepared to investigate the dielectric relaxation, ferroelectric, piezoelectric properties, and temperature stability. The starting materials are PbO (Ishihara, 99.9%), ZrO_2 (Ishihara, 99.9%), TiO_2 (Ishihara, 99.9%), Y_2O_3 (Alfa Aesar, 99.9%), Bi_2O_3 (Alfa Aesar, 99.9%), Sb_2O_5 (Alfa Aesar, 99.8%), and Mn_2O_3 (Alfa Aesar, 99%).

The powders were weighed and mixed through ball milling, with partially stabilized zirconia balls as media, in alcohol for 12 h. After drying, the mixture was calcined in a covered alumina crucible at 850 °C for 2 h. The calcined powder is then ball-milled for 12 h. Dried powder is sieved and pressed into pellets using polyvinyl alcohol (PVA: 5%) as a binder at a pressure of 100 MPa in 5 mm of diameter. Pellets were sintered at 1200 °C for 2 h in a sealed alumina crucible. To minimize PbO loss, a PbO-rich atmosphere was maintained by placing powders of $PbZrO_3$ inside the crucible used as packing

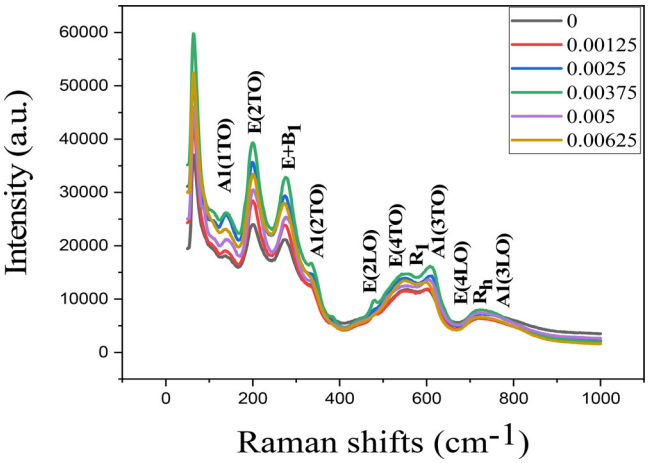

Figure 1. Raman spectra of $Pb_{1-x}Y_{x/2}Bi_{x/2}[(Zr_{0.53}\ Ti_{0.47})_{0.92} - (Mn_{1/3}\ Sb_{2/3})_{0.08}]O_3$ ceramics for x = 0, 0.00125, 0.0025, 0.00375, 0.005 and 0.00625 at room temperature.

powders. Afterward the samples were polished and coated with silver paint as electrodes for the property measurement. Finally, to ensure the contact between the electrodes and ceramic surfaces well, the samples were heat-treated at 750 °C for 10 min.

The crystalline structure of the ceramics was examined using X–ray diffraction (XRD) analysis with CuK_α radiation (PANalytical X'pert PRO, Phillips, Eindhoven, the Netherlands) and Raman spectrometry (Microscopes Spectrometer, Renishaw, Gloucestershire, UK). The microstructure was observed using a scanning electron microscope (SEM) (FESEM, Quanta 250FEG, USA). The densities of the sintered specimens were measured by a water-immersion method using Archimedes-principle.

The dielectric permittivity was measured as a function of temperature using a multi-frequency LCR meter (4284 A, Agilent, Santa Clara, CA, USA). The piezoelectric properties were measured after samples were polarized in silicon oil and aged in air for 24 h. For investigation of the piezoelectric properties, the resonant and anti-resonant frequencies were measured by an Impedance Analyzer (Agilent 4294 A).

3. Results and discussion

3.1. Raman spectra and XRD patterns

Raman spectroscopy is sensitive to the symmetry of crystal- line structures and thus is used to further study the structure and the phase evolution of ceramics. Figure 1 shows the room temperature Raman spectra recorded in the 50–1000 cm^{-1} wave number range of $Pb_{1-x}Y_{x/2}Bi_{x/2}[(Zr_{0.53}\ Ti_{0.47})_{0.92}-(Mn_{1/3}\ Sb_{2/3})_{0.08}]O_3$ ceramics for x = 0, 0.00125, 0.0025, 0.00375, 0.005 and 0.00625. The spectra show peaks around 204, 265, 325, 558, 706, and 759 cm^{-1}, matching well with the typical Raman peaks for perovskite PZT [47, 48]. Each peak represents the Raman active vibrational mode for a given sample, suggesting that the samples are pure and do not contain any compositional inhomogeneity.

Raman scattering analysis is an effective method for detecting the degree of structural disorder, such as tetragonal and rhombohedral phases in PZT-based systems near the MPB [18, 49–52]. As the ferroelectric state below the Curie temperature, three cubic

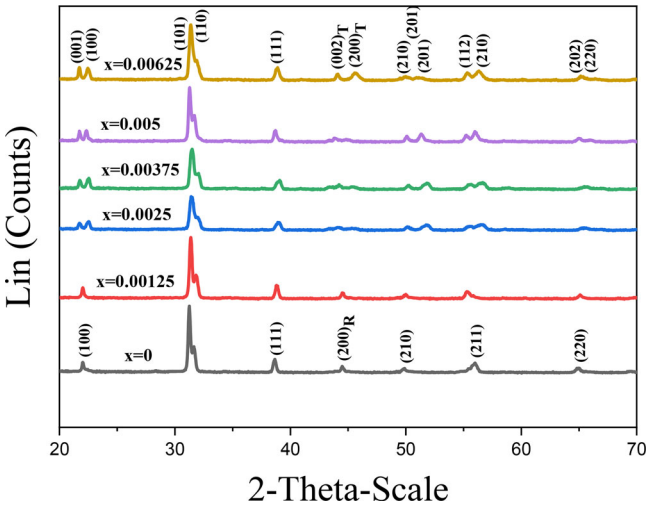

Figure 2. Powder X-ray diffraction pattern of PYBZT-PMS ceramics at room temperature.

T_{1u} modes are transformed as the A_1+E modes in both tetragonal and rhombohedral symmetry. The T_{2u} mode is transformed as the B_1+E (silent) mode in tetragonal or rhombohedral symmetry and the E mode in rhombohedral symmetry. Moreover, the distinguishable Raman features during the rhombohedral–tetragonal phase transition can be easily presented in the low and high Raman shifts (wave numbers) regions.

In the Raman shifts range of 130–480 cm^{-1}, five peaks appear for both the rhombohedral and tetragonal structures. The intensity of peak in the coexisting tetragonal and rhombohedral structure is assigned to be the E(2TO (transversal optic)). The A_1(1TO), silent (E + B_1), A_1(2TO) and E(2LO (longitudinal optic)) modes correspond to the tetragonal or rhombohedral structures. As the Raman shifts are in the high range of 500–900 cm^{-1}, the tetragonal and rhombohedral phases can be easily observed by their variations of A_1(3TO), A_1(3LO), E(4TO), E(4LO), R_1, and R_h modes. The tetragonal A_1(3TO) mode located at about 598 cm^{-1}, tetragonal E(4TO) mode at 556 cm^{-1}, and the Rhombohedral R_1 mode at about 574 cm^{-1} are all generated transverse (O–B–O bending) modes from T_{1u}(3) transformation. Similarly, the tetragonal A_1(3LO) and E(4LO) modes at about 780 and 717 cm^{-1} and the rhombohedral R_h mode at 725 cm^{-1} are the generated longitudinal (B–O stretching) transformation of T_{1u}(3).

The intensities of the tetragonal mode E (2TO) increase with the increment of x content in the studied ceramic system, which means that the transformation of the rhombohedral phase to the tetragonal phase takes place [53]. However, R_h rhombohedral intensities are decreasing, which is also indicative of presumption of the transformation of the rhombohedral phase into a tetragonal phase, whereas samples containing x = 0.0025, 0.00375 and 0.005 indicate the coexistence of a tetragonal phase and a phase rhombohedric competition E (2TO) and Rh with moderate intensities.

The X-ray diffraction patterns of PYBZT-PMS ceramics containing various Y^{3+} and Bi^{3+} amounts (x = 0, 0.00125, 0.0025, 0.00375, 0.005 and 0.00625) sintered at 1200 °C for 2 h are shown in Fig. 2. The XRD patterns confirm that all the PYBZT-PMS powders are pure in nature, and free from the pyrochlore phases.

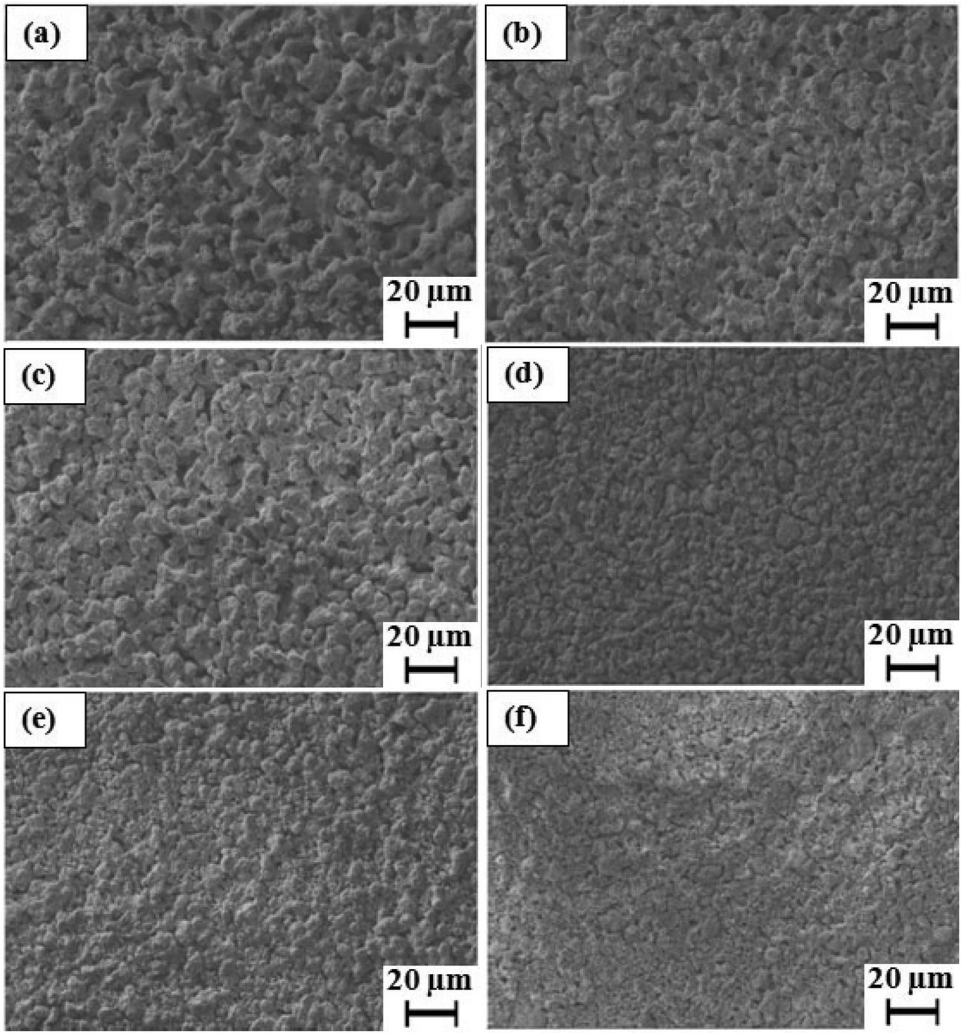

Figure 3. SEM micrographs of PYBZT-PMS ceramics prepared with different concentrations [(a) $x = 0$, (b) $x = 0.00125$, (c) $x = 0.0025$, (d) $x = 0.00375$, (e) $x = 0.005$, (f) $x = 0.00625$].

The tetragonal (T), rhombohedral (R) and tetragonal–rhombohedral phases are identified by analysis of peaks [002 (tetragonal), 200 (tetragonal), 200 (rhombohedral)] in 2θ range of 43°–47°. The result shows that typical coexistence of both rhombohedral and tetragonal phase [$(0\ 0\ 2)_T$, $(2\ 0\ 0)_R$ and $(2\ 0\ 0)_T$] is observed at room temperature when the YB content is $0.0025 \leq x \leq 0.005$, and the rhombohedral phase $(2\ 0\ 0)_R$ can be obtained when YB content is $x \leq 0.00125$. The structure of solid solution transforms from coexistence of both rhombohedral and tetragonal phase to tetragonal phase $(0\ 0\ 2)_T$ and $(2\ 0\ 0)_T$ when YB content is $x \geq 0.00625$.

The smaller ionic radius of Y^{3+} (0.90 Å) and Bi^{3+} (0.103 Å), compared to that of Pb^{2+} (1.19 Å) promotes the phase transformation from rhombohedral to tetragonal. The MPB composition is expected to affect the piezoelectric and dielectric properties.

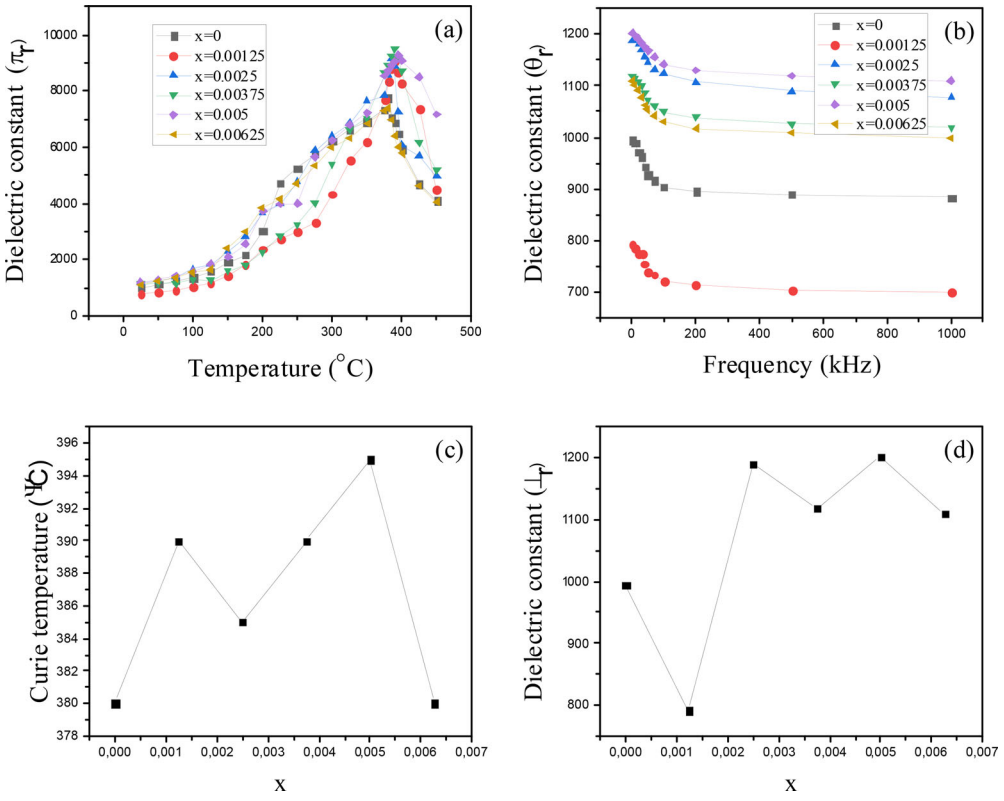

Figure 4. Dielectric constant-temperature spectra (a) measured at 1 kHz, dielectric constant-frequency spectra (b), Curie temperature-x spectra (c), and dielectric constant-x spectra (d) for PYBZT-PMS ceramics at room temperature.

3.2. Microstructure of ceramics

The scanning electron micrographs of PYBZT-PMS with x = 0, 0.00125, 0.0025, 0.00375, 0.005 and 0.00625 sintered at 1200 °C for 2 h are shown in Fig. 3(a)–(f). It is observed that the micrographs are uniform. Hence, it is assumed that the ceramic filler is uniformly distributed in the PZT-PMS matrix.

It can be seen that the morphology of the different samples under probe appears to be very dense, the porosity decreases and the grain size decreased with the increasing amount addition of Y^{3+} and Bi^{3+} ions. No pyramidal grains were observed, indicating the absence of undesirable pyrochlore phases, which validates the XRD results, reported above.

3.3. Electric properties

Figure 4(a) shows the temperature dependence of the dielectric constant (ε_r) according to Y and Bi substitution (x = 0, 0.00125, 0.0025, 0.00375, 0.005 and 0.00625) of the PYBZT-PMS ceramics samples measured at 1 kHz from room temperature up to 450 °C.

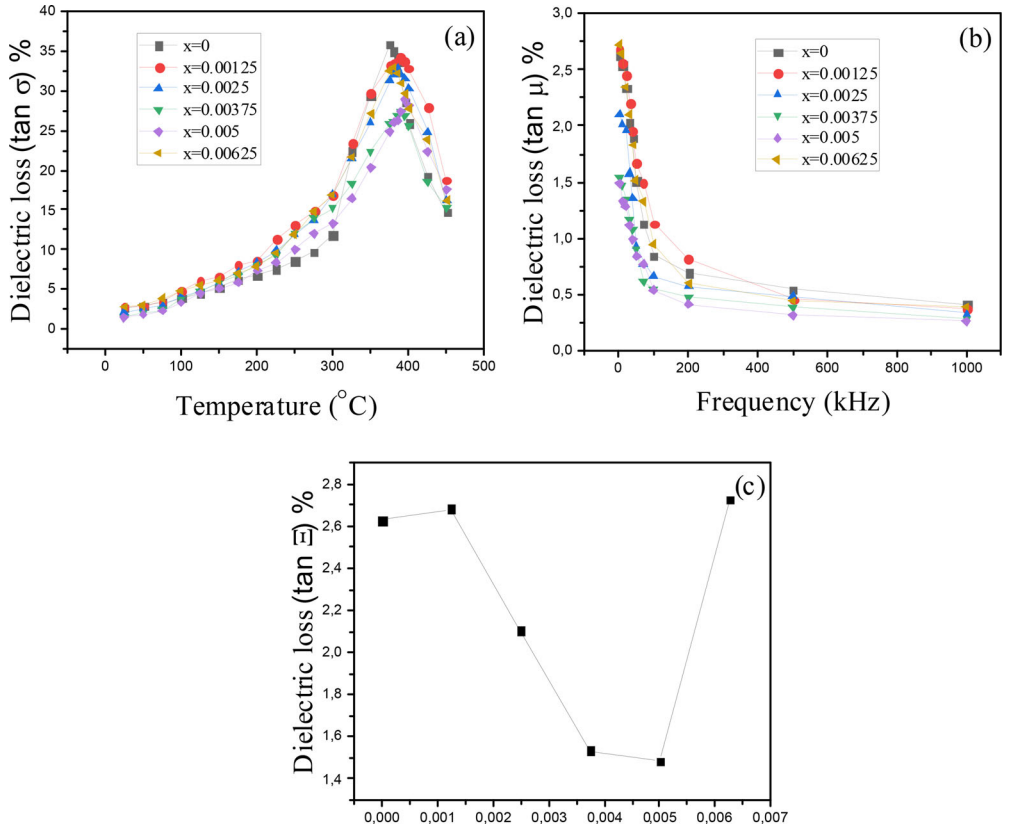

Figure 5. (a) Temperature dependence of dielectric loss (tan δ) measured at 1 kHz, (b) plots of tan δ versus frequency and (c) plots of tan δ versus *x*, for PYBZT-PMS ceramics.

It can be seen from Fig. 4(a) that ε_r increase with increasing temperature up to a particular temperature called T_c (Curie temperature), and then reduces. The maximum dielectric constant (ε_{max}) was obtained at Curie temperature (T_c). At T_c, the appearance of peaks indicates the phase transition of the compounds from the ferroelectric phase to paraelectric phase [54, 55].

The plot of dielectric constant versus frequency of $Pb_{1-x}Y_{x/2}Bi_{x/2}[(Zr_{0.53}Ti_{0.47})_{0.92}-(Mn_{1/3}Sb_{2/3})_{0.08}]O_3$ for $x = 0$, 0.00125, 0.0025, 0.00375, 0.005, and 0.00625 samples at room temperature are shown in Fig. 4(b). It can be seen that the dielectric constant decreases with increasing of frequency i.e. he dielectric constant has a maximum value at the lowest frequency and then decreases with the increase in the frequency of the sample. At low frequency, all types of polarizations (ionic, electronic, dipole and space charges polarization) contribute to the dielectric constant. At higher frequencies, the easy depolarization of dipoles that exist at weak bonded interface and boundary regions results in small value of dielectric constant. At higher frequency, only orientation polarization contributes to the dielectric constant [56].

Figure 4(c) shows the temperature of maximum dielectric constant T_c varies with x addition. T_c increased gradually with the content of x increased (up to a value of $x \leq 0.005$), they are 380, 390, 385, 390, 395 °C, respectively, then reduced to a content of $x = 0.00625$ (380 °C).

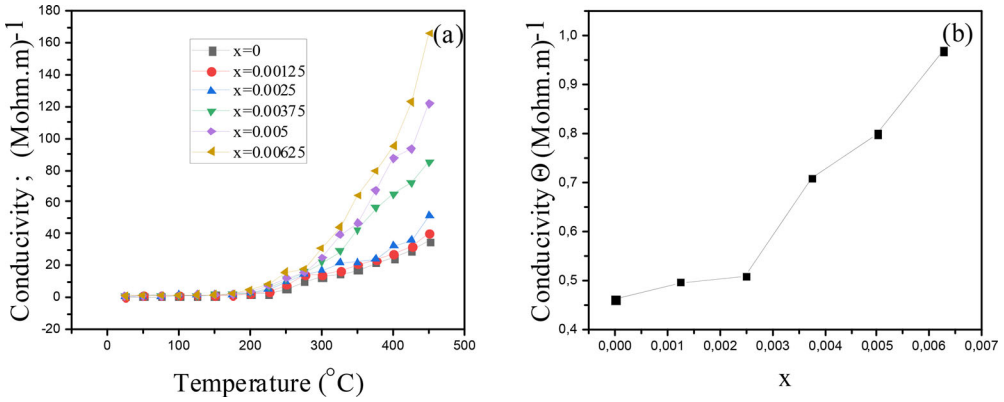

Figure 6. Electrical conductivity as a function of: (a) temperature, (b) x content, for PYBZT-PMS ceramics.

Figure 4(d) shows the dielectric constant (ε_r) of the specimens according to x at room temperature. The dielectric constant showed the maximum value of 1201 at $x = 0.005$ and then decreased.

The specimen having composition $x = 0.005$ shows maximum value of dielectric constant (ε_{max}) which is 9279 near T_c. Additionally, the substitution of Y and Bi into PYBZT-PMS ceramics slightly increases the transition temperature from 380 °C ($x = 0$) to 395 °C ($x = 0.005$) which is quite high and may be useful in technical applications. The reason for the improvement in dielectric properties and deterioration in microstructural for the composition $x = 0.005$ may be attributed to the fact that the composition is very close to the morphotropic phase boundary (MPB) [57, 58].

Figure 5(a) shows the temperature dependence of the dielectric loss (tan δ) for PYBZT-PMS ceramics with various Y_2O_3, Bi_2O_3 content measured at 1 kHz, for the test temperature range from room temperature to 450 °C. For the all compositions sintered at 1200 °C, the plot of tan δ versus temperature, just before the phase transition, an increase (and then decrease) in the dielectric loss is observed this is characteristic of PZT type ceramics. This increase in tan δ may be due to an increase in the electrical conduction of the residual current and absorption current [59, 60]. The dielectric loss is a contribution of conduction loss due to ions migration, ions jump, also ion polarization and vibration loss. It can be seen that all PYBZT-PMS ceramics exhibit a dielectric loss < 0.4.

Figure 5(b) shows the variation of dielectric loss tan δ of all the samples at different frequencies measured at room temperature. In all the samples, the dielectric loss decreases with the increase of frequencies. Dielectric loss decreases with the increase in frequency and, has the lowest value around at 1000 kHz. The interfacial dipoles cannot orient themselves in the direction of the alternating field with the increase in frequency. So charges can no longer follow the field and their contribution to the dielectric constant deceases [60, 61].

Figure 5(c) shows the tan δ of the $Pb_{1-x}Y_{x/2}Bi_{x/2}[(Zr_{0.53}\ Ti_{0.47})_{0.92}$–$(Mn_{1/3}\ Sb_{2/3})_{0.08}]O_3$ ceramics ($x = 0$, 0.00125, 0.0025, 0.00375, 0.005, and 0.00625) as a function of x measured at 1 kHz and at room temperature. When the content of $x \leq 0.00125$, tan δ increased with the content of x increased. When the content of x was $0.0025 \leq x \leq 0.005$, tan δ decreased

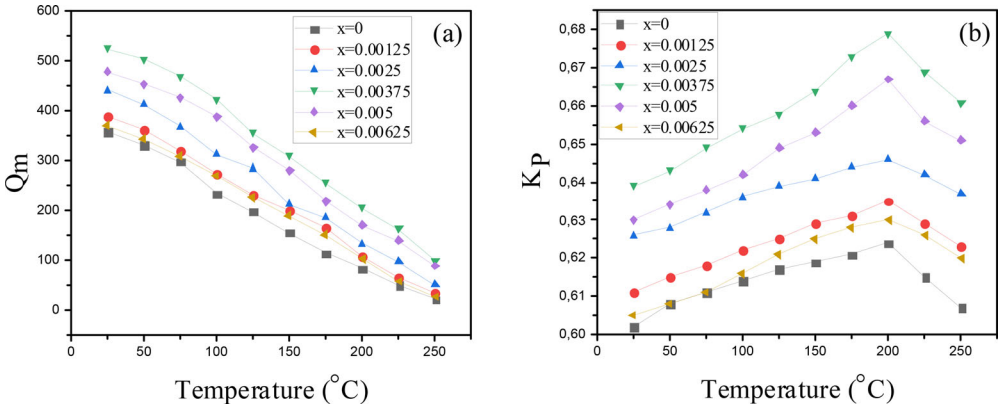

Figure 7. Temperature dependence of Q_m (a) and K_P (b) of the PYBZT-PMS ceramics sintered at 1200 °C measured at 1 kHz.

gradually with the content of x increased and then increased with the content of $x > 0.005$. It is reported that the higher densification can lower the dielectric loss of ceramics [62–65]. Thus, the lowest tan δ of PYBZT-PMS ceramic is because of the highest bulk density at $x = 0.0025$, 0.00375 and 0.005.

The temperature-dependent electrical conductivity σ of PYBZT-PMS ceramics are shown in Fig. 6(a) with $x = 0$, 0.00125, 0.0025, 0.00375, 0.005, and 0.00625. It is measured in a wide temperature range from 25 °C to 450 °C and at 1 kHz. The results show that σ is observed to increase with the increasing of temperature. From room temperature to around 350 °C, slow growth in the σ value occurs. Above a temperature of 350 °C, a significant increase in the σ value is observed. The high activation energy value at high temperature is due to the thermally activated charge carriers.

The electrical conductivity of all samples as a function of x content at room temperature are showed in Fig. 6(b). The results indicate that PYBZT-PMS ceramics show an increase in electrical conductivity with increasing x content. When the content x increases have a much more conductive path of continuous conduct network that allows electrons to pass through.

Figure 7 shows the temperature dependence of the mechanical quality factor Q_m and the electromechanical coupling factor K_P of $Pb_{1-x}Y_{x/2}Bi_{x/2}[(Zr_{0.53}\ Ti_{0.47})_{0.92}-(Mn_{1/3}Sb_{2/3})_{0.08}]O_3$ ceramics.

It is shown from Fig. 7(a) that the mechanical quality factor Q_m value of the PYBZT-PMS ceramics continuously decreased with increasing temperature. When the temperature shifts from 25 °C to 450 °C, the Q_m values of all samples showed an obvious decrease. The addition of positive and low-valent metal ions by adding acceptor impurities greatly increases the negative charge center and carrier holes in the ceramic body, which generates a large amount of space charge [66, 67]. The negative space charge accumulates at the positive end of the domain, while positive space charge accumulates at the negative end of the domain wall, forming a space charge field in the same direction as the original polarization of the electric domain, which will inhibit domain wall motion [67, 68]. With the increase of temperature, the space charge migrates into the ceramic body, which reduces the accumulation of space charge and promotes the movement of domain wall. For the soft PZT materials, the amount of space charge generated

Table 1. summarizes the density, porosity and lattice parameters (a, b, c), for all the investigated compounds.

				Lattice parameters			
					Crystal system (tetragonal)		
x content	Measured density ρ (g/cm^3)	Relative density (%)	Porosity	Crystal system (rhombohedral) a = b = c (Å)	a = b (Å)	c (Å)	c/a
x = 0	7,49	93.62	0.06375	4.0392	–	–	–
x = 0.00125	7.58	94.75	0.0525	4.0504	–	–	–
x = 0.0025	7.74	96.75	0.0325	4.0613	4.0462	4.1243	1.0193
x = 0.00375	7.82	97.75	0.0225	4.0782	4.0673	4.1272	1.0147
x = 0.005	7.76	97	0.03	4.0656	4.0524	4.1258	1.0181
x = 0.00625	7.55	94.37	0.05625	–	4.0328	4.1236	1.0225

Table 2. The mechanical quality factor Q_m, the electromechanical coupling factor K_P, the piezoelectric charge constant d_{31}, the piezoelectric voltage constant g_{31} and the Young modulus Y of PYBZT-PMS ceramics sintered at 1200 °C.

x	Q_m	K_P	d_{31} (10^{-12} C/N)	g_{31} (10^{-3} m V/N)	Y (10^{10} N/m^2)
0	358.499	0.602	57.68	9.45	7.884
0.00125	389.756	0.611	59.888	9.937	8.438
0.0025	441.967	0.626	63.587	10.667	9.632
0.00375	525.232	0.639	68.698	11.349	11.058
0.005	479.365	0.63	65.687	10.896	10.157
0.00625	370.442	0.605	61.534	9.884	8.153

in the ceramic body is small, and the change of temperature causes the small amount of space charge migration.

As shown in Fig. 7(b), the electromechanical coupling factor K_P value of the PYBZT-PMS ceramics increase initially and then decrease drastically with the increasing temperature. It can be seen that K_P of PYBZT-PMS ceramics keeps stable when the temperature below 200 °C. This result further reveals that PYBZT-PMS ceramics is a promising candidate for high temperature piezoelectric applications.

All the piezoelectric properties of the $Pb_{1-x}Y_{x/2}Bi_{x/2}[(Zr_{0.53}\ Ti_{0.47})_{0.92}$–$(Mn_{1/3}\ Sb_{2/3})_{0.08}]O_3$ ceramics with x = 0, 0.00125, 0.0025, 0.00375, 0.005, and 0.00625 measured at 1 kHz and at room temperature, are listed in Table 2.

4. Conclusions

In summary, $Pb_{1-x}Y_{x/2}Bi_{x/2}[(Zr_{0.53}\ Ti_{0.47})_{0.92}$–$(Mn_{1/3}\ Sb_{2/3})_{0.08}]O_3$ (x = 0, 0.00125, 0.0025, 0.00375, 0.005, 0.00625) piezoelectric ceramics were prepared by a conventional solid-state sintering method and studied systematically by means of Raman spectra, XRD, SEM and electrical measurements. Raman Spectra and XRD revealed that the PYBZT-PMS ceramics were of pure perovskite structure with the coexistence of tetragonal and rhombohedral phase (MPB) was observed for x = 0.0025–0.005. Addition of Y_2O_3 and Bi_2O_3 leads to a decrease in grain size and promotes bulk density of the ceramics. The electrical conductivity σ measurement presented that with the increasing of temperature and x content, the σ of the PYBZT-PMS ceramics increased. The conduction behavior can be described by the intrinsic charge carriers conduction mechanism and extrinsic semiconductor conductive mechanism in different temperature range. When x = 0.00375, it exhibits optimum electrical performance: ε_r = 1119.397,

$\tan\delta = 0.01535$, $T_c = 390\,^{\circ}C$, $\rho = 7.82\,g/cm^3$, $\sigma = 0.709$ (Mohm m)$^{-1}$, $Q_m = 525.232$, $K_P = 0.639$, $d_{31} = 68.698 \times 10^{-12}$ C/N, $g_{31} = 11.349 \times 10^{-3}$ m V/N and $Y = 11.058 \times 10^{10}$ N/m^2. These results confirm that the ceramic is with the potentialities to be applied in multilayer ceramic capacitors and electro-strictive actuators.

References

[1] A. J. Moulson and J. M. Herbert, *Electroceramics: Materials, Properties, Applications*, 2nd ed. (Wiley, New York, 2003).

[2] G. H. Haertling, Ferroelectric ceramics: history and technology, *J. Am. Ceram. Soc.* **82** (4), 797 (1999). DOI: 10.1111/j.1151-2916.1999.tb01840.x.

[3] X. Yuhan, *Ferroelectric Materials and Their Applications* (Elsevier, Amsterdam, 1991).

[4] B. Jaffe, W. R. Cook, and H. Jaffe, *Piezoelectric Ceramics* (Academic Press, London, 1971).

[5] P. Kour *et al.*, Electrical properties of calcium modified PZT (52/48) ceramics, *Solid State Commun.* **190**, 33 (2014). DOI: 10.1016/j.ssc.2014.03.025.

[6] F. Kahoul *et al.*, Study of dielectric and piezoelectric properties of (1-x)PZT-xSFN ceramics prepared by conventional solid state reaction method, *J. Chem. Soc. Pak.* **42** (5), 634 (2020).

[7] R. Guo *et al.*, Origin of the high piezoelectric response in $PbZr_{1-x}Ti_xO_3$, *Phys. Rev. Lett.* **84** (23), 5423 (2000). DOI: 10.1103/PhysRevLett.84.5423.

[8] M. R. Soares, A. M. R. Senos, and P. Q. Mantas, Phase coexistence region and dielectric properties of PZT ceramics, *J. Eur. Ceram. Soc.* **20** (3), 321 (2000). DOI: 10.1016/S0955-2219(99)00170-3.

[9] A. S. Bhalla, R. Guo, and E. F. Alberta, Some comments on the morphotropic phase boundary and property diagrams in ferroelectric relaxor systems, *Mater. Lett.* **54** (4), 264 (2002). DOI: 10.1016/S0167-577X(01)00575-4.

[10] A. Boutarfaia, Investigations of co-existence region in lead zirconate-titanate solid solutions: X-ray diffraction studies, *Ceram. Int.* **26** (6), 583 (2000). DOI: 10.1016/S0272-8842(99)00099-1.

[11] J. Joseph *et al.*, Structural investigations on $Pb(Zr_xTi_{1-x})O_3$ solid solutions using the X-ray Rietveld method, *J. Mater. Sci.* **35** (6), 1571 (2000). DOI: 10.1023/A:1004778223721.

[12] M. Ahart *et al.*, Origin of morphotropic phase boundaries in ferroelectrics, *Nature* **451** (7178), 545 (2008). DOI: 10.1038/nature06459.

[13] A. G. Khachaturyan, Ferroelectric solid solutions with morphotropic boundary: rotational in stability of polarization, metastable coexistence of phases and nanodomain adaptive states, *Philos. Mag.* **90** (1–4), 37 (2010). DOI: 10.1080/14786430903074789.

[14] S. P. Singh *et al.*, A study of phase coexistence and temperature dependent monoclinic to tetragonal phase transition in the multiferroic (1-x)$Pb(Fe_{1/2}\ Nb_{1/2})\ O_3$-x$PbTiO_3$ ($x = 0.08$), *Appl. Phys. Lett.* **97** (12), 122902 (2010). DOI: 10.1063/1.3486159.

[15] B. Noheda *et al.*, A monoclinic ferroelectric phase in the $Pb(Zr_{1-x}Ti_x)O_3$ solid solution, *Appl. Phys. Lett.* **74** (14), 2059 (1999). DOI: 10.1063/1.123756.

[16] B. Noheda and D. E. Cox, Bridging phases at the morphotropic boundaries of lead oxide solid solutions, *Phase. Transit.* **79** (1–2), 5 (2006). DOI: 10.1080/01411590500467262.

[17] B. Noheda *et al.*, Tetragonal-to-monoclinic phase transition in a ferroelectric perovskite: the structure of $PbZr_{0.52}Ti_{0.48}O_3$, *Phys. Rev. B* **61** (13), 8687 (2000). DOI: 10.1103/PhysRevB.61.8687.

[18] B. Noheda *et al.*, Stability of the monoclinic phase in the ferroelectric perovskite $PbZr_{1-x}Ti_xO_3$, *Phys. Rev. B* **63** (1), 014103 (2000). DOI: 10.1103/PhysRevB.63.014103.

[19] V. Tiwari and G. Srivastava, The effect of Li_2CO_3 addition on the structural, dielectric and piezoelectric properties of PZT ceramics, *Ceram. Int.* **41** (2), 2774 (2015). DOI: 10.1016/j.ceramint.2014.10.096.

[20] Ragini *et al.*, Room temperature structure of $Pb(Zr_xTi_{1-x})O_3$ around the morphotropic phase boundary region: a Rietveld study, *J. Appl. Phys.* **92** (6), 3266 (2002). DOI: 10.1063/1.1483921.

[21] B. V. Hiremath, A. I. Kingon, and J. V. Biggers, Reaction sequence in the formation of lead zirconate-lead titanate solid solutions: role of raw materials, *J. Am. Ceram. Soc.* **66** (11), 790 (1983). DOI: 10.1111/j.1151-2916.1983.tb10564.x.

[22] A. Kumar and S. K. Mishra, Dielectric, piezoelectric, and ferroelectric properties of lanthanum-modified PZTFN ceramics, *Int. J. Miner. Metall. Mater.* **21** (10), 1019 (2014). DOI: 10.1007/s12613-014-1003-9.

[23] F. Kahoul *et al.*, Dielectric, phase structure, microstructure, and dielectric properties of $(1-x)Pb(Zr_{0.50}\ Ti_{0.50})O_3-xBa(W_{2/3}\ Mn_{1/3})O_3$ ceramics, *Ferroelectrics* **572** (1), 229 (2021). DOI: 10.1080/00150193.2020.1868885.

[24] D. Damjanovic, Ferroelectric, dielectric and piezoelectric properties of ferroelectric thin films and ceramics, *Rep. Prog. Phys.* **61** (9), 1267 (1998). DOI: 10.1088/0034-4885/61/9/002.

[25] A. Kumar *et al.*, Poling electric field dependent domain switching and piezoelectric properties of mechanically activated $(Pb_{0.92}La_{0.08})(Zr_{0.60}Ti_{0.40})O_3$ ceramics, *J. Mater. Sci.: Mater. Electron.* **26** (6), 3757 (2015). DOI: 10.1007/s10854-015-2899-1.

[26] L. Yang *et al.*, Mechanism of grain growth and excellent polarization, dielectric relaxtion of La^{3+}, Nd^{3+} modified PZT nano-films prepared by sol–gel technique, *J. Mater. Sci.: Mater. Electron.* **29** (21), 18011 (2018). DOI: 10.1007/s10854-018-9974-3.

[27] S. Takahashi, Effects of impurity doping in lead zirconate-titanate ceramics, *Ferroelectrics* **41** (1), 143 (1982). DOI: 10.1080/00150198208210617.

[28] Y. D. Hou *et al.*, Effect of MnO_2 addition on the structure and electrical properties of $Pb(Zn_{1/3}Nb_{2/3})_{0.20}(Zr_{0.50}Ti_{0.50})_{0.80}O_3$ ceramics, *J. Am. Ceram. Soc.* **87** (5), 847 (2004). DOI: 10.1111/j.1551-2916.2004.00847.x.

[29] Y. D. Hou *et al.*, Structure and electrical properties of PMZN-PZT quaternary ceramics for piezoelectric transformers, *Sens. Actuator, A* **116** (3), 455 (2004). DOI: 10.1016/j.sna.2004.05.012.

[30] M. P. Zheng *et al.*, Effect of valence state and incorporation site of cobalt dopants on the microstructure and electrical properties of 0.2PZN–0.8PZT ceramics, *Acta Mater.* **61** (5), 1489 (2013). DOI: 10.1016/j.actamat.2012.11.026.

[31] M. I. Morozov and D. Damjanovic, Charge migration in $Pb(Zr,Ti)O_3$ ceramics and its relation to ageing, hardening and softening, *J. Appl. Phys.* **107** (3), 034106 (2010). DOI: 10.1063/1.3284954.

[32] N. Horchidan *et al.*, A comparative study of hard/soft PZT-based ceramic composites, *Ceram. Int.* **42** (7), 9125 (2016). DOI: 10.1016/j.ceramint.2016.02.179.

[33] V. S. Kathavate *et al.*, Role of domain configurations on the mechanistic modeling of indentation size effects (ISE) in nanohardness of hard and soft PZT piezoceramics, *Int. J. Adv. Eng. Sci. Appl. Math.* **13** (1), 63 (2021). DOI: 10.1007/s12572-020-00279-1.

[34] V. D. Kugel and L. E. Cross, Behavior of soft piezoelectric ceramics under high sinusoidal electric fields, *J. Appl. Phys.* **84** (5), 2815 (1998). DOI: 10.1063/1.368422.

[35] G. H. Haertling and C. E. Land, Hot-pressed $(Pb,La)(Zr,Ti)O_3$ ferroelectric ceramics for electrooptic applications, *J. Am. Ceram. Soc.* **54** (1), 1 (1971). DOI: 10.1111/j.1151-2916.1970.tb12105.x-i1.

[36] L. Pdungsap *et al.*, Optimized conditions for fabrication of La-dopant in PZT ceramics, *Sens. Actuator, A* **122** (2), 250 (2005). DOI: 10.1016/j.sna.2005.06.002.

[37] M. Hinterstein *et al.*, Influence of lanthanum doping on the morphotropic phase boundary of lead zirconate titanate, *J. Appl. Phys.* **108** (2), 024110 (2010). DOI: 10.1063/1.3437399.

[38] G. Viola *et al.*, Effect of grain size on domain structures, dielectric and thermal depoling of Nd-substituted bismuth titanate ceramics, *Appl. Phys. Lett.* **103** (18), 182903 (2013). DOI: 10.1063/1.4827537.

[39] T. M. Kamel and G. d. With, Grain size effect on the poling of soft Pb(Zr,Ti)O_3 ferroelectric ceramics, *J. Eur. Ceram. Soc.* **28** (4), 851 (2008). DOI: 10.1016/j.jeurceramsoc.2007.08.010.

[40] L. Zhang *et al.*, The effect of poling condition on the piezoelectric properties of 0.3PNN-0.7PZT ceramics in the vicinity of MPB, *J. Mater. Sci.: Mater. Electron.* **23** (3), 688 (2012). DOI: 10.1007/s10854-011-0472-0.

[41] A. Kumar *et al.*, Optimization of poling parameters of mechanically processed PLZT 8/60/40 ceramics based on dielectric and piezoelectric studies, *Eur. Phys. J. B* **88** (11), 287 (2015). DOI: 10.1140/epjb/e2015-60414-9.

[42] M. J. Hoffmann *et al.*, Correlation between microstructure, strain behavior, and acoustic emission of soft PZT ceramics, *Acta Mater.* **49** (7), 1301 (2001). DOI: 10.1016/S1359-6454(01)00025-8.

[43] H. Li *et al.*, Microstructure and piezoelectric properties of NaF-doped $K_{0.5}Na_{0.5}Nb_{0.95}Ta_{0.05}O_3$ lead-free ceramics, *J. Mater. Sci.* **48** (3), 1396 (2013). DOI: 10.1007/s10853-012-6887-z.

[44] H. Liu *et al.*, Structure evolution and electrical properties of Y^{3+}-doped $Ba_{1-x}Ca_xZr_{0.07}Ti_{0.93}O_3$ ceramics, *J. Am. Ceram. Soc.* **97** (7), 2076 (2014). DOI: 10.1111/jace.12900.

[45] A. Kumar, K. C. J. Raju, and A. R. James, Micro-structural, dielectric, ferroelectric and piezoelectric properties of mechanically processed $(Pb_{1-x}La_x)(Zr_{0.60}Ti_{0.40})O_3$ ceramics, *J. Mater. Sci.: Mater. Electron.* **29** (16), 13483 (2018). DOI: 10.1007/s10854-018-9473-6.

[46] Z. G. Zhu *et al.*, Dielectric and electrical conductivity properties of PMS-PZT ceramics, *J. Am. Ceram. Soc.* **89** (2), 717 (2006). DOI: 10.1111/j.1551-2916.2005.00750.x.

[47] A. G. S. Filho *et al.*, Raman scattering study of the $PbZr_{1-x}Ti_xO_3$ system: rhombohedral-monoclinic-tetragonal phase transitions, *Phys. Rev. B* **66** (13), 132107 (2002). DOI: 10.1103/PhysRevB.66.132107.

[48] J. Frantti *et al.*, Effect of A and B-cation substitutions on the phase stability of $PbTiO_3$ ceramics, *Phys. Rev. B* **59** (1), 12 (1999). DOI: 10.1103/PhysRevB.59.12.

[49] Z. Xia and Q. Li, Phase transformation in (0.9-x)$Pb(Mg_{1/3}Nb_{2/3})O_3$-$PbTiO_3$-0.10$PbZrO_3$ piezoelectric ceramics: X-ray diffraction and Raman investigation, *Solid State Commun.* **142** (6), 323 (2007). DOI: 10.1016/j.ssc.2007.03.004.

[50] H. Zhang *et al.*, Phase transition revealed by Raman spectroscopy in screen-printed lead zirconate titanate thick films, *J. Appl. Phys.* **76** (7), 4294 (1994). DOI: 10.1063/1.357314.

[51] M. K. Zhu *et al.*, Analysis of phase coexistence in Fe_2O_3-doped 0.2PZN–0.8PZT ferroelectric ceramics by Raman scattering spectra, *J. Am. Ceram. Soc.* **89** (12), 3739 (2006). DOI: 10.1111/j.1551-2916.2006.01281.x.

[52] C. C. Tsai *et al.*, The phase structure, electrical properties, and correlated characterizations of (Mn, Sb) co-tuned PZMnNS–PZT ceramics with relaxation behavior near the morphotropic phase boundary, *Ceram. Int.* **40** (8), 11713 (2014). DOI: 10.1016/j.ceramint.2014.03.185.

[53] A. Meklid *et al.*, Phase structure, microstructure and electrical properties of PCNS–PZ–PT ternary ceramics near the morphotropic phase boundary, *Appl. Phys. A* **126** (1), 32 (2020). DOI: 10.1007/s00339-019-3209-1.

[54] B. Behera, P. Nayak, and R. N. P. Choudhary, Dielectric anomaly in $LiCa_2V_5O_{15}$ ceramics, *Mater. Lett.* **61** (18), 3859 (2007). DOI: 10.1016/j.matlet.2006.12.048.

[55] B. Tiwari, T. Babu, and R. N. P. Choudhary, Dielectric response of Mn and Ce substituted PZT ferroelectric ceramics, *Mater. Today: Proceed* **43** (1), 535 (2021). DOI: 10.1016/j.matpr.2020.12.032.

[56] S. K. Pradhan *et al.*, Tuning of dielectric and impedance properties of PVDF by incorporation of Mg doped PZT, *J. Mater. Sci.: Mater. Electron.* **29** (19), 16842 (2018). DOI: 10.1007/s10854-018-9779-4.

[57] K. Ramam and K. Chandramouli, Dielectric and piezoelectric properties of combinatory effect of A-site isovalent and B-site acceptor doped PLZT ceramics, *Ceram. Silik.* **53** (3), 189 (2009).

[58] A. Kumar, V. Pal, and S. K. Mishra, Preparation, microstructure, dielectric and electrical analysis of Fe-modified PZT piezoceramics, *J. Mater. Sci.: Mater. Electron.* **32** (3), 2946 (2021). DOI: 10.1007/s10854-020-05046-3.

[59] B. Tareev, *Physics of Dielectric Materials* (Mir Publisher, Moscow, 1979).

[60] H. Menasra *et al.*, Structural and electrical characterization of La^{3+} substituted PMS-PZT (Zr/Ti: 60/40) ceramics, *Mater. Sci. Poland* **36** (1), 1 (2018). DOI: 10.1515/msp-2018-0033.

[61] A. A. M. Farag *et al.*, Electrical conductivity, dielectric properties and optical absorption of organic based nanocrystalline sodium copper chlorophyllin for photodiode application, *J. Alloys Compd.* **513**, 404 (2012). DOI: 10.1016/j.jallcom.2011.10.058.

[62] S. J. Penn *et al.*, Effect of porosity and grain size on the microwave dielectric properties of sintered alumina, *J. Am. Ceram. Soc.* **80** (7), 1885 (2005). DOI: 10.1111/j.1151-2916.1997.tb03066.x.

[63] R. A. Dorey, S. B. Stringfellow, and R. W. Whatmore, Effect of sintering aid and repeated sol infiltrations on the dielectric and piezoelectric properties of a PZT composite thick film, *J. Eur. Ceram. Soc.* **22** (16), 2921 (2002). DOI: 10.1016/S0955-2219(02)00062-6.

[64] Y. Guo, K. Kakimoto, and H. Ohsato, Structure and electrical properties of lead-free $(Na_{0.5}K_{0.5})NbO_3$-$BaTiO_3$ Ceramics, *Jpn. J. Appl. Phys.* **43** (9B), 6662 (2004). DOI: 10.1143/JJAP.43.6662.

[65] C. Jianchao *et al.*, Phase structure, microstructure and electrical properties of $K_xNa_{(1-x)}NbO_3$ piezoelectric ceramics with different K/Na ratio, *J. Wuhan Univ. Technol.-Mat. Sci. Edit.* **34** (1), 30 (2019). DOI: 10.1007/s11595-019-2010-5.

[66] M. Takahashi, Space charge effect in lead zirconate titanate ceramics caused by the addition of impurities, *Jpn. J. Appl. Phys.* **9** (10), 1236 (1970). DOI: 10.1143/JJAP.9.1236.

[67] Z. Z. Du *et al.*, Electrical properties and temperature stability of CeO_2 and $MnCO_3$ co-doped $Pb_{0.95}Sr_{0.05}(Mn_{1/3}Nb_{2/3})_{0.05}$ $(Zr_{0.48}Ti_{0.52})_{0.95}O_3$ piezoceramics with high mechanical quality factor, *J. Mater. Sci.: Mater. Electron.* **32** (3), 2895 (2021). DOI: 10.1007/s10854-020-05042-7.

[68] S. Takahashi and M. Takahashi, Effects of impurities on the mechanical quality factor of lead zirconate titanate ceramics, *Jpn. J. Appl. Phys.* **11** (1), 31 (1972). DOI: 10.1143/JJAP.11.31.